Article:

Akerib, D.S., Alsum, S., Araújo, H.M. et al. (93 more authors) (2025) Nuclear recoil calibration at Sub-keV energies in LUX and its impact on dark matter search sensitivity. Physical Review Letters, 134 (6). 061002. ISSN 0031-9007

https://doi.org/10.1103/physrevlett.134.061002

Nuclear Recoil Calibration at Sub-keV Energies in LUX and Its Impact on Dark Matter Search Sensitivity

D.S. Akerib,[1,2] S. Alsum,[3] H.M. Araújo,[4] X. Bai,[5] J. Balajthy,[6] J. Bang,[7] A. Baxter,[8] E.P. Bernard,[9] A. Bernstein,[10] T.P. Biesiadzinski,[1,2] E.M. Boulton,[9,11,12] B. Boxer,[8] P. Brás,[13] S. Burdin,[8] D. Byram,[14,15] M.C. Carmona-Benitez,[16] C. Chan,[7] J.E. Cutter,[6] L. de Viveiros,[16] E. Druszkiewicz,[17] A. Fan,[1,2] S. Fiorucci,[11,7] R.J. Gaitskell,[7] C. Ghag,[18] M.G.D. Gilchriese,[11] C. Gwilliam,[8] C.R. Hall,[19] S.J. Haselschwardt,[20] S.A. Hertel,[21,11] D.P. Hogan,[9] M. Horn,[15,9] D.Q. Huang,[7,*] C.M. Ignarra,[1,2] R.G. Jacobsen,[9] O. Jahangir,[18] W. Ji,[1,2] K. Kamdin,[9,11] K. Kazkaz,[10] D. Khaitan,[17] E.V. Korolkova,[22] S. Kravitz,[11] V.A. Kudryavtsev,[22] E. Leason,[23] K.T. Lesko,[11] J. Liao,[7] J. Lin,[9] A. Lindote,[13] M.I. Lopes,[13] A. Manalaysay,[11,6] R.L. Mannino,[24,3] N. Marangou,[4] D.N. McKinsey,[9,11] D.-M. Mei,[14] J.A. Morad,[6] A.St.J. Murphy,[23] A. Naylor,[22] C. Nehrkorn,[20] H.N. Nelson,[20] F. Neves,[13] A. Nilima,[23] K.C. Oliver-Mallory,[4,9,11] K.J. Palladino,[3] C. Rhyne,[7] Q. Riffard,[9,11] G.R.C. Rischbieter,[25] P. Rossiter,[22] S. Shaw,[20,18] T.A. Shutt,[1,2] C. Silva,[13] M. Solmaz,[20] V.N. Solovov,[13] P. Sorensen,[11] T.J. Sumner,[4] N. Swanson,[7] M. Szydagis,[25] D.J. Taylor,[15] R. Taylor,[4] W.C. Taylor,[7] B.P. Tennyson,[12] P.A. Terman,[24] D.R. Tiedt,[19] W.H. To,[26] L. Tvrznikova,[9,11,12] U. Utku,[18] A. Vacheret,[4] A. Vaitkus,[7] V. Velan,[9] R.C. Webb,[24] J.T. White,[24] T.J. Whitis,[1,2] M.S. Witherell,[11] F.L.H. Wolfs,[17] D. Woodward,[16] X. Xiang,[7] J. Xu,[10] and C. Zhang[14]

[1]*SLAC National Accelerator Laboratory, 2575 Sand Hill Road, Menlo Park, CA 94205, USA*
[2]*Kavli Institute for Particle Astrophysics and Cosmology, Stanford University, 452 Lomita Mall, Stanford, CA 94309, USA*
[3]*University of Wisconsin-Madison, Department of Physics, 1150 University Ave., Madison, WI 53706, USA*
[4]*Imperial College London, High Energy Physics, Blackett Laboratory, London SW7 2BZ, United Kingdom*
[5]*South Dakota School of Mines and Technology, 501 East St Joseph St., Rapid City, SD 57701, USA*
[6]*University of California Davis, Department of Physics, One Shields Ave., Davis, CA 95616, USA*
[7]*Brown University, Department of Physics, 182 Hope St., Providence, RI 02912, USA*
[8]*University of Liverpool, Department of Physics, Liverpool L69 7ZE, UK*
[9]*University of California Berkeley, Department of Physics, Berkeley, CA 94720, USA*
[10]*Lawrence Livermore National Laboratory, 7000 East Ave., Livermore, CA 94551, USA*
[11]*Lawrence Berkeley National Laboratory, 1 Cyclotron Rd., Berkeley, CA 94720, USA*
[12]*Yale University, Department of Physics, 217 Prospect St., New Haven, CT 06511, USA*
[13]*LIP-Coimbra, Department of Physics, University of Coimbra, Rua Larga, 3004-516 Coimbra, Portugal*
[14]*University of South Dakota, Department of Physics, 414E Clark St., Vermillion, SD 57069, USA*
[15]*South Dakota Science and Technology Authority, Sanford Underground Research Facility, Lead, SD 57754, USA*
[16]*Pennsylvania State University, Department of Physics, 104 Davey Lab, University Park, PA 16802-6300, USA*
[17]*University of Rochester, Department of Physics and Astronomy, Rochester, NY 14627, USA*
[18]*Department of Physics and Astronomy, University College London, Gower Street, London WC1E 6BT, United Kingdom*
[19]*University of Maryland, Department of Physics, College Park, MD 20742, USA*
[20]*University of California Santa Barbara, Department of Physics, Santa Barbara, CA 93106, USA*
[21]*University of Massachusetts, Amherst Center for Fundamental Interactions and Department of Physics, Amherst, MA 01003-9337 USA*
[22]*University of Sheffield, Department of Physics and Astronomy, Sheffield, S3 7RH, United Kingdom*
[23]*SUPA, School of Physics and Astronomy, University of Edinburgh, Edinburgh EH9 3FD, United Kingdom*
[24]*Texas A & M University, Department of Physics, College Station, TX 77843, USA*
[25]*University at Albany, State University of New York, Department of Physics, 1400 Washington Ave., Albany, NY 12222, USA*
[26]*California State University Stanislaus, Department of Physics, 1 University Circle, Turlock, CA 95382, USA*

Dual-phase xenon time projection chamber (TPC) detectors offer heightened sensitivities for dark matter detection across a spectrum of particle masses. To broaden their capability to low-mass dark matter interactions, we investigated the light and charge responses of liquid xenon (LXe) to sub-keV nuclear recoils. Using neutron events from a pulsed Adelphi Deuterium-Deuterium neutron generator, an *in situ* calibration was conducted on the LUX detector. We demonstrate direct measurements of light and charge yields down to 0.45 keV and 0.27 keV, respectively, both approaching single quanta production, the physical limit of LXe detectors. These results hold significant implications for the future of dual-phase xenon TPCs in detecting low-mass dark matter via nuclear recoils.

Introduction.—Dual-phase xenon time projection chambers (TPCs), a leading technology for dark matter detection[1–4], measure nuclear recoils (NR) from weakly interacting massive particles (WIMPs) through both scintillation light (S1) and ionization charge (S2) in liquid xenon (LXe). Detecting low-mass dark matter remains challenging due to limited calibrations of low-energy NR responses. This study presents the first simultaneous measurements of light (L_y) and charge (Q_y) yields for NR in LXe, characterizing the average quanta per keV down to the sub-keV region using the Large Underground Xenon (LUX) detector. These yields were obtained indirectly by comparing data with simulation of the NR spectrum.

Data Collection and Analysis.—In 2016, we enhanced the NR calibration of the LUX detector [5] *in situ*, using neutron events from a pulsed Adelphi[1] Deuterium-Deuterium (D-D) neutron generator.[2] LUX has a 250 kg active mass and 122 2-inch PMTs in top and bottom arrays, shielded by a 7.6 m × 6.1 m cylindrical water tank. Incident particles generate immediate S1 scintillation photons, detected by PMTs with a gain (g_1) of 0.096 ± 0.003 photon detected (phd)/photon [9, 10]. Concurrently, the ionization charge drifts upwards in LXe and, upon transitioning to the gas phase, produces the S2 signal with an ionization gain (g_2) of 18.5 ± 0.9 phd/electron. Each electron induces, on average, 25.72 ± 0.04 phd with a width of 5.47 ± 0.03 phd across PMTs [11]. For LUX details, consult [6, 7, 9, 12–19].

A schematic of the experimental setup is depicted in Fig. 1. We directed a collimated neutron beam (2.45 MeV) through a conduit of 377 cm length and 4.9 cm diameter. The conduit center is 10 cm below the LXe surface, within a 50 cm deep active volume. The D-D generator operated at a 250 Hz frequency and a 20 µs pulse width, producing an instantaneous flux of 2.8×10^8 neutrons/s. At this flux rate, on average, about 0.06 neutrons reach the TPC with each pulse, resulting in a probability of approximately 3% for multiple neutron interactions per pulse. In the pulsed mode, the D-D generator's trigger time provides an estimate of the neutron interaction time in the TPC, enabling us to study low-energy events that produce detectable ionization signals without accompanying scintillation signals.

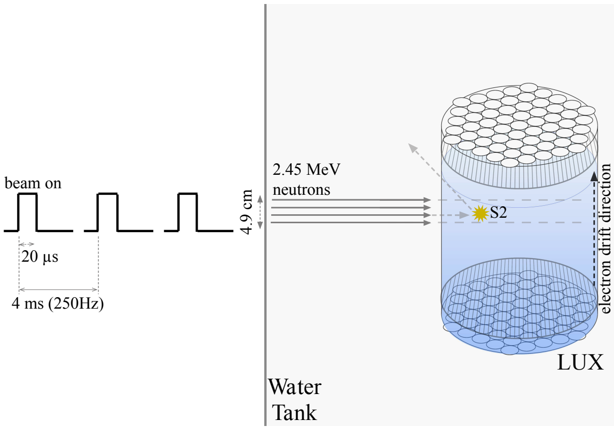

FIG. 1. Diagram (not to scale) of the LUX's short-pulsed D-D neutron calibration.

For yield measurements, we selected D-D neutron events that exhibited a single scatter, characterized by one observed S2 exceeding 44 phd; signals below this threshold are notably affected by spurious background single electrons (SE). This criterion may encompass neutron multi-scatters, where one S2 exceeds the threshold and others do not, we address this potential systematics in our signal modeling. Targeting low-energy neutron-induced xenon recoils, we permitted events with zero or one preceding S1 pulse to the S2. In this context, an S1, unlike those in other LUX analyses, is defined as a scintillation signal without the typical two-fold coincidence, with its magnitude quantified by the discrete photon counts on the PMTs, termed 'spikes' [9]. S2 signals must occur within 65 to 125 µs after a D-D trigger, align with the neutron conduit depth (7.5-12.5 cm), and be located within the neutron beam's xy projection, defined as a 7 cm diameter cylinder, to capture the majority of signal events while eliminating spurious coincidences. For events with S1, a time cut of > 2.5 µs between S1 and S2 further refines our selection, eliminating events where S1 pulses are misconstrued from the leading edge of an S2. To maximize event inclusion, we abstain from a radial fiducialization cut. Notably, S2 signal charge loss near the TPC wall is deemed negligible (0.13% of events) [11], attributed to charge accumulation on the wall, guiding signals inward during vertical transit [13].

The primary background in this study stems from electron-train (e-train) events, ubiquitous in xenon TPCs. Defined as sequences of single or clustered few-electron emissions trailing large S2 pulses with roughly 10 ms time constants [20], these e-trains may be mistakenly identified as S2 signals from low-energy neutron interactions, complicating the calibration process. Utilizing the temporal precision of the D-D trigger to require coincidence with the TPC signals effectively eliminates prevalent e-train background interference. Two additional quiet-time cuts further diminish e-train contamination: the first mandates a 4 ms hiatus between LUX-triggered events and the candidate signal, and the second asserts that no SE emissions precede the observed S2 within the event. Both cuts, optimized for signal-to-noise ratio, reduce e-train events by factors of three and two,

---

[1] Adelphi Technology Inc., 2003 E. Bayshore Road, Redwood City, CA 94063

[2] For the first LUX D-D neutron calibration (LUX DD2013) details, see [6–8].

respectively, with 80% signal acceptance. The ‘no-SE-ahead-S2’ cut, however, might inadvertently exclude genuine events that exhibit SE from low-energy neutron interactions, potentially compromising signal uptake. This bias will be addressed in subsequent modeling. Moreover, the D-D trigger facilitates *in situ* evaluations of the lingering e-train event rate by probing TPC events where the S2 appears before the D-D trigger pulse, as shown in Fig. 2 (top panel). The background rate for events featuring a D-D neutron S1 but lacking a corresponding S2, which instead coincide with e-train S2s, is quantified using the NEST2.0 model [21]. This background predominantly affects the lowest-energy bins and is continuously updated along with the NEST2.0 yield models when fitting the signal model to the data, which will be discussed later.

Random small S1s, primarily photoelectron (PHE) pulses from PMT dark counts or subsequent to high energy depositions in the TPC [20], pose major challenges in accurately identifying signal events with 0-spike and 1-spike S1s. The average background PHE rate is 1.8 ± 0.1 within 1-ms event windows, complicating data interpretation. For instance, a coincidental PHE pulse aligning with a 0-spike event could cause the event to be misinterpreted as a 1-spike event. Additionally, within genuine 1-spike events, extraneous background PHEs can give the appearance of multiple 1-spike S1 pulses preceding the primary S2 signal. Unlike the uniform temporal distribution of background PHEs, genuine 1-spike S1 signals from D-D neutron interactions are concentrated within a narrowly defined D-D S1 window prior to S2 emergence. This temporal distinction, coupled with D-D trigger timing, enables us to statistically distinguish between signal events and accidentals, and to discern between 0-spike and 1-spike S1 signal events by analyzing their collective temporal distributions. For details, see Sec. 6.3.4 in [11].

Upon completing the event selection and background analysis, we determined the absolute rates for D-D neutron single elastic scatter events with S1 spanning $0, 1, 2, 3, 4, 5$ spikes. Figure 2 (bottom panel) showcases the S2 spectra corresponding to each S1 (represented by black data points). S2 pulse areas, for events with S1 ≥ 2 spikes, are corrected for position-dependent detection efficiency using a ^{83m}Kr calibration. This correction is not implemented to S2s associated with 0 and 1-spike S1s due to the lack of accurate z-position information, resulting from either the absence of S1 signals or confusion caused by background PHEs. For consistency, the same treatment of the S2 pulse area is applied in the signal modeling.

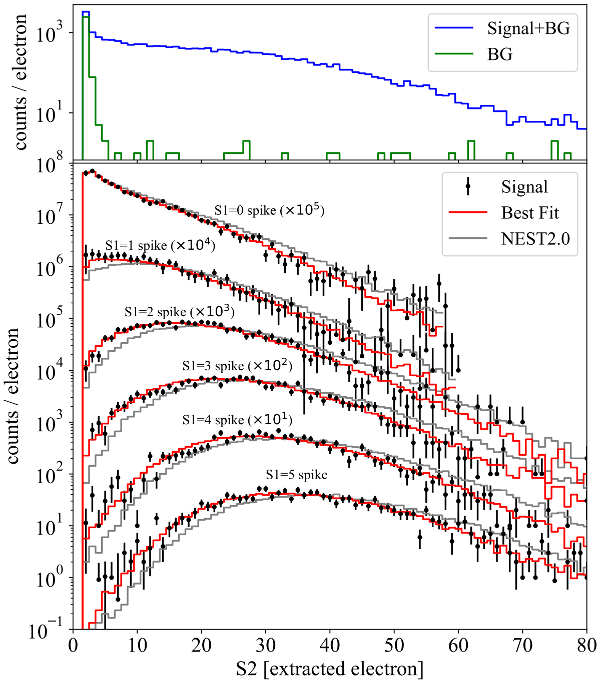

FIG. 2. Top panel: The blue histogram shows the combined S2 spectrum of data for S1 values ranging from 0 to 5 spikes. The green histogram represents the measured background from events where the S2 precedes the D-D trigger pulse within the same dataset. Bottom panel: Background-subtracted S2 spectra corresponding to S1 spikes of 0 to 5 are shown as black points. The red histograms represent the best-fit results, while the gray ones are produced from the original NEST2.0 yield models. For display purposes, both measured and modeled S2 spectra for S1 $= i$ spike have been scaled by a factor of 10^{5-i}, where $i = 0, 1, 2, 3, 4, 5$. Histogram bins and error bars for black data points extending into the negative domain have been suppressed.

Signal Modeling.—To model the differential NR spectra arising from single elastic scatter interactions of neutrons at low energies, we conducted a GEANT4-based simulation, which fully incorporates the LUX geometry, including the LUX water tank and the D-D neutron conduit (LUXSim [22]). In this simulation, we exclusively select neutron events involving either elastic scattering or neutron capture [3], while vetoing any events with gamma-ray energy depositions. For each simulated neutron event, we record the four highest-energy deposition vertices, capturing crucial details such as neutron and deposited energies, along with their (x, y, z) positions. This dataset enabled us to model systematic effects related to event selection criteria, including the S2 threshold and the ‘no-SE-ahead-S2’ cut, as well as the merging of adjacent S2 pulses in the vertical direction.

During this calibration, the LUX active volume exhibited a notably non-uniform electric field [13]. To account for this field variation, a dedicated field model [24] was specifically developed for the calibration period. This field model is utilized to calculate the electric field strength at each recorded vertex. Since our analysis is

---

[3] Radiative neutron capture by xenon isotopes results in finite NR energy deposition (up to 0.3 keV) in LXe [11, 23].

carried out in the observed space, we employ the same field model to map each simulated vertex from real space into observed space. The weighted average of the electric field for selected neutron events is 400 ± 80 V/cm.

A LUX-adapted NEST2.0 program is employed to simulate the production and detection of S1 and S2 signals for each recorded vertex, utilizing information derived from deposited energy, electric field strength, and position. At the core of NEST2.0 lie the empirically-derived L_y and Q_y models. The recoil interaction initially generates N_{ex} excitons (Xe*) and N_{i} electron-ion ($\mathrm{e}^-\mathrm{Xe}^+$) pairs at the interaction site. These excitations subsequently de-excite or recombine, resulting in the production of S1 and S2 signals. The fluctuations in N_{ex} and N_{i} are independently modeled using Gaussian statistics, with widths (σ) determined by $\sqrt{F\mathrm{N}_{\mathrm{ex}}}$ and $\sqrt{F\mathrm{N}_{\mathrm{i}}}$, respectively, within NEST2.0. Here, F represents a Fano-like factor. While the value of F is consistent with 1 based on DD2013 [6, 7] and the XENON10 AmBe calibration [25], it carries a significant uncertainty due to the absence of mono-energetic lines in NR calibrations. The treatment of F is discussed in the next section.

LUX detector parameters were measured *in situ* for the calibration period [11, 26]. A single photon would lead to 1.17 PHE and the single PHE resolution is 1.00 ± 0.46. Other measured parameters include the SE mean pulse area and width, and g_1 and g_2 as presented earlier. These parameters were incorporated into NEST2.0 for simulating signal detection processes. Following signal detection modeling, we combined any two S2 signals in a simulated neutron event with a z separation of < 2 µs (D-D neutron S2 1–99% width) in drift time. To determine the S1 to D-D trigger time for each vertex, we sampled it from a time distribution directly measured from data and added it to the drift time of each vertex, obtaining the S2 to D-D trigger time. The S2 trigger efficiency of the data acquisition system, measured from a separate D-D calibration dataset [27], was applied to S2s in each simulated event for event triggering. We corrected the S2 pulse area of surviving events with S1 ≥ 2 spikes to match real data. Additionally, we evaluated S1 pulse finding and classification efficiencies as functions of size through visual assessment of 6000 events using calibration data. These measured efficiencies were applied to simulated events for consistency with real data. All simulated events underwent the same event selection criteria as real data. The resulting signal model is presented in Fig. 2 (gray histograms). A noticeable discrepancy between the calibration data and the original signal model was observed, which may be attributed to the limited constraints on yields at very low energies from [6, 7], the primary basis for NEST2.0 yield models.

Yield Measurements.—Following detailed signal modeling, we adjusted the light yield (L_y) and charge yield (Q_y) models within NEST2.0—both shapes and amplitudes down to 0 keV—simultaneously yet independently, to achieve the best fit to the calibration data (Fig. 2) using the least squares method:

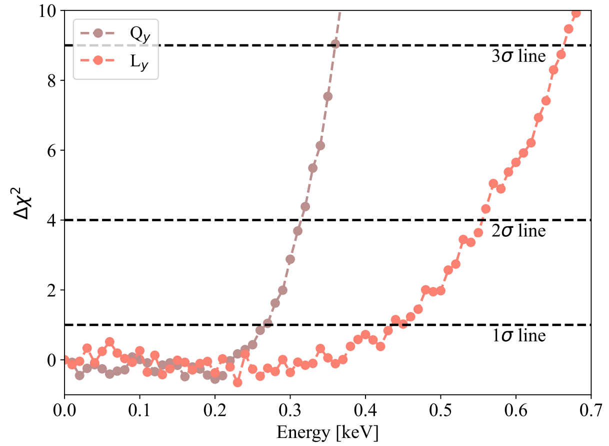

FIG. 3. Evaluated $\Delta\chi^2$ values as a function of energy. The lowest energies to which these calibration data are sensitive to for L_y and Q_y are 0.45 ± 0.03 keV and 0.27 ± 0.04 keV at 1-σ sensitivity level, respectively. At 2-σ level, L_y 0.56 ± 0.02 keV, Q_y 0.31 ± 0.03 keV; and at 3-σ level, L_y 0.66 ± 0.02 keV, Q_y 0.35 ± 0.03 keV.

$$\chi^2 = \sum_{i=1}^{N} \frac{(O_i - E_i)^2}{E_i},$$

where O_i and E_i are the observed and simulated counts per bin, and N is the total number of valid bins across the six spectra. The shape adjustments primarily focus on the low-energy end (< 3 keV), as the high-energy end is well constrained by DD2013 [6]. The L_y primarily affects the relative counts and shapes of the six S2 spectra, whereas Q_y influences their shapes. The parametrization of the yield models is illustrated in Figure 8.7 and 8.8 of [11]. In the simultaneous fitting of these six S2 spectra, we employ a single overall event rate normalization factor to enforce a robust constraint. This factor is intentionally left free to ensure conservativeness. The Fano-like factor F is used to adjust the S2 spectrum widths in the signal model. It is treated as a free parameter in the fitting due to its unknown uncertainty. This conservative approach also captures other secondary factors contributing to the signal distribution widths. The best fit is achieved with $\chi^2 = 246.0$ for 262 degrees of freedom (N_{dof}) and 8 parameters. The χ^2/N_{dof} values for the S1 $= 0$, 1, 2, 3, 4, and 5 spike S2 spectra are 41.9/36, 17.1/30, 47.1/38, 53.2/43, 39.3/31, and 47.4/44, respectively. The fitting results indicate a positive correlation between L_y and Q_y. Uncertainties on both L_y and Q_y are conservatively determined by marginalizing over all other fitting parameters, capturing the effects of their mutual correlation within the fit. As g_1 and g_2 are in direct degeneracy with both L_y and Q_y for the observed S1

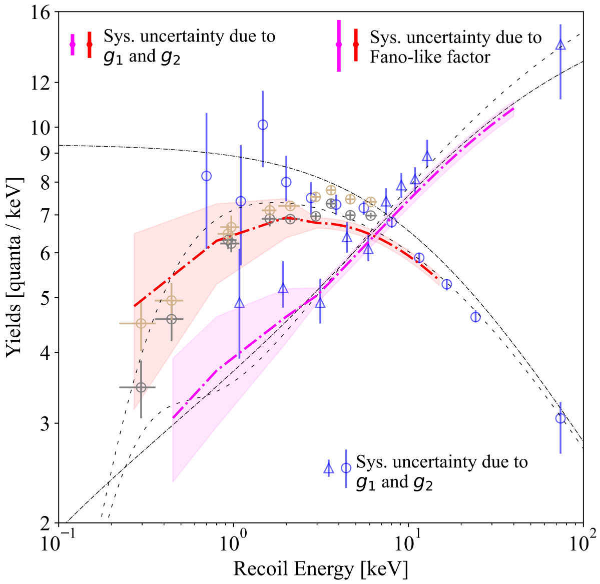

FIG. 4. L_y (magenta) and Q_y (red) measurements for DD2016 at 400 V/cm are shown with statistical uncertainties (light bands). Q_y results from XeNu 2019 at 220 V/cm (gray) and 550 V/cm (golden) [28], and DD2013 at 180 V/cm (light blue triangles for L_y, circles for Q_y) are included. NEST2.0 and NEST2.3.11 models at 400 V/cm are shown as black dash-dotted and dashed lines, respectively. Code to extract and implement the DD2016 results is available at `https://gitlab.com/huangdq2017/implementation_of_lux_dd_yields`.

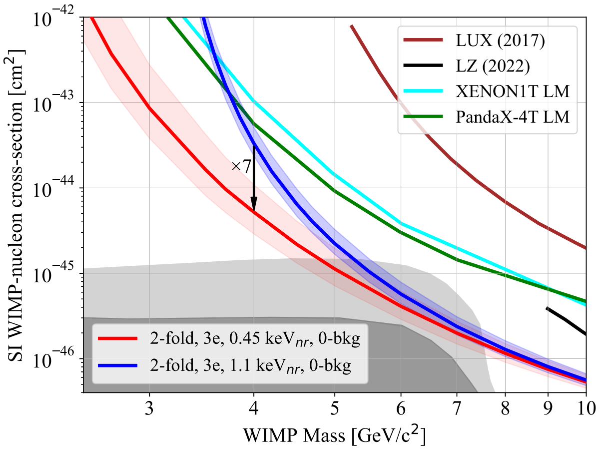

FIG. 5. The projected 90% sensitivities for a background-free LXe experiment with LZ-SR1 [4] exposure are shown as red and blue curves for different energy thresholds, with uncertainty bands reflecting yield uncertainties. The searches use both scintillation and ionization channels with a 2-fold coincidence requirement and a three extracted-electron threshold. The curves demonstrate the low-mass WIMP search sensitivity improvement due to the lower NR energy threshold obtained in this work. For reference, limits from LUX (2017) (brown)[13], XENON1T (2021) low-mass (LM) WIMP search (cyan)[32], PandaX-4T (2023) LM WIMP search (green)[33], and LZ (2022) (black)[4] are also shown. The gray regions represent the neutrino floors for the baseline scenario (light) and after reducing solar flux uncertainties by a factor of 10 (dark) [34].

and S2 distributions, we assess the contributions of their non-negligible uncertainties to the yield measurements by repeating the fitting using g_1 and g_2 values at their 1-σ uncertainty levels. For details, see Sec. 8.2 in [11].

To establish the lowest energies to which this calibration data is sensitive for L_y and Q_y, we independently evaluate them based on the best-fit yield models. This involves cutting off the corresponding yield (assume zero yield) below certain energies from the best-fit yield model and calculating the $\Delta\chi^2$ values concerning the case of no energy cutoff in the signal model against the calibration data. The results, along with 1-σ, 2-σ, and 3-σ sensitivity lines, are shown in Fig. 3. We report the lowest energies that the data are sensitive to for both L_y and Q_y at the 1-σ sensitivity level, yielding L_y and Q_y measurements of 0.45 ± 0.03 keV and 0.27 ± 0.04 keV, respectively, representing the lowest-energy NR calibrations in LXe to date. The final L_y and Q_y measurements of this work (DD2016) are presented in Fig. 4.

With both L_y and Q_y measurements, we can constrain the Lindhard model [29, 30], which describes the quenching of electronic excitation from NR in LXe. The Lindhard factor k is measured to be 0.146 ± 0.013, assuming a constant W value (energy required to produce a scintillation or ionization quantum) of 13.7 eV [31]. This value is consistent with the standard Lindhard model prediction of 0.166 within 1.5-σ.

Impact on WIMP search and beyond.—This work allows us to estimate the potential sensitivity of an optimized dual-phase xenon TPC to low-mass WIMP interactions within the standard halo model [35]. Figure 5 demonstrates the gain in sensitivity for low-mass WIMP dark matter, benefiting from the improvements in the calibration of signal yields presented here. The limit curves are generated using NEST2.3.11 [36], with light and charge yield models matching this work. The search includes both S1 and S2 channels, with a two-fold PMT coincidence requirement and a three extracted-electron threshold. A background-free 0.9 tonne-year exposure, equivalent to the LZ-SR1 exposure [4], is assumed. Zero WIMP acceptance is enforced for recoil energies below 0.45 keV and 1.1 keV, corresponding to the lowest yield measurements of this work and [6], respectively. Sensitivity improvements greater than a factor of ×7 are achieved for WIMP masses below 4 GeV/c^2. A thorough investigation of detector accidental coincidence backgrounds, combined with leveraging the double-PHE effect [37, 38], is necessary to achieve S1 and S2 thresholds at this level. As xenon TPCs improve in sensitivity for dark matter detection, lowering the energy threshold toward the Solar Boron-8 neutrino floor becomes increasingly critical [32, 33, 39, 40]. This work also broadens the application of dual-phase TPCs to other rare event searches, such as coherent elastic neutrino-nucleus scattering from reactor antineutrinos [41] and probing a potential nonzero neutrino magnetic moment [42]. Additionally, achieving near-single-quantum sensitivity in both light and charge yields marks a significant technological milestone, offering deeper insights into noble liquid microphysics.

This work was partially supported by the U.S. Department of Energy (DOE) under Award No. DE-AC02-05CH11231, DE-AC05-06OR23100, DE-AC52-07NA27344, DE-FG01-91ER40618, DE-FG02-08ER41549, DE-FG02-11ER41738, DE-FG02-91ER40674, DE-FG02-91ER40688, DE-FG02-95ER40917, DE-NA0000979, DE-SC0006605, DE-SC0010010, DE-SC0015535, and DE-SC0019066; the U.S. National Science Foundation under Grants No. PHY-0750671, PHY-0801536, PHY-1003660, PHY-1004661, PHY-1102470, PHY-1312561, PHY-1347449, PHY-1505868, and PHY-1636738; the Research Corporation Grant No. RA0350; the Center for Ultra-low Background Experiments in the Dakotas (CUBED); and the South Dakota School of Mines and Technology (SDSMT). Laboratório de Instrumentação e Física Experimental de Partículas (LIP)-Coimbra acknowledges funding from Fundação para a Ciência e a Tecnologia (FCT) through the Project-Grant PTDC/FIS-NUC/1525/2014. Imperial College and Brown University thank the UK Royal Society for travel funds under the International Exchange Scheme (IE120804). The UK groups acknowledge institutional support from Imperial College London, University College London, the University of Sheffield, and Edinburgh University, and from the Science & Technology Facilities Council for PhD studentships R504737 (EL), M126369B (NM), P006795 (AN), T93036D (RT) and N50449X (UU). This work was partially enabled by the University College London (UCL) Cosmoparticle Initiative. The University of Edinburgh is a charitable body, registered in Scotland, with Registration No. SC005336. This research was conducted using computational resources and services at the Center for Computation and Visualization, Brown University, and also the Yale Science Research Software Core. We gratefully acknowledge the logistical and technical support and the access to laboratory infrastructure provided to us by SURF and its personnel at Lead, South Dakota. SURF was developed by the South Dakota Science and Technology Authority, with an important philanthropic donation from T. Denny Sanford. SURF is a federally sponsored research facility under Award Number DE-SC0020216.

---

[*] Corresponding Author:dongqing_huang@alumni.brown.edu

[1] D.S. Akerib *et al.* (LUX), “Results from a search for dark matter in the complete LUX exposure,” Phys. Rev. Lett. **118**, 021303 (2017), arXiv:1608.07648 [astro-ph.CO].
[2] E. Aprile *et al.* (XENON), “Dark Matter Search Results from a One Ton-Year Exposure of XENON1T,” Phys. Rev. Lett. **121**, 111302 (2018), arXiv:1805.12562 [astro-ph.CO].
[3] Yue Meng *et al.* (PandaX-4T), “Dark Matter Search Results from the PandaX-4T Commissioning Run,” Phys. Rev. Lett. **127**, 261802 (2021), arXiv:2107.13438 [hep-ex].
[4] J. Aalbers *et al.* (LZ), “First Dark Matter Search Results from the LUX-ZEPLIN (LZ) Experiment,” Phys. Rev. Lett. **131**, 041002 (2023), arXiv:2207.03764 [hep-ex].
[5] D. S. Akerib *et al.* (LUX Collaboration), “The Large Underground Xenon (LUX) Experiment,” Nucl. Instrum. Methods **A704**, 111–126 (2013).
[6] D. S. Akerib *et al.* (LUX Collaboration), “Low-energy (0.7-74 kev) nuclear recoil calibration of the lux dark matter experiment using d-d neutron scattering kinematics,” (2016), arXiv:1608.05381 [physics.ins-det].
[7] James R Verbus, An Absolute Calibration of Sub-1 keV Nuclear Recoils in Liquid Xenon Using D-D Neutron Scattering Kinematics in the LUX Detector, Ph.D. thesis, Brown University (2016).
[8] J. R. Verbus *et al.*, “Proposed low-energy absolute calibration of nuclear recoils in a dual-phase noble element TPC using D-D neutron scattering kinematics,” Nucl. Instrum. Meth. **A851**, 68–81 (2017), arXiv:1608.05309 [physics.ins-det].
[9] D. S. Akerib *et al.* (LUX Collaboration), “Improved limits on scattering of weakly interacting massive particles from reanalysis of 2013 LUX data,” Phys. Rev. Lett. **116**, 161301 (2016).
[10] C.H. Faham, V.M. Gehman, A. Currie, A. Dobi, P. Sorensen, and R.J. Gaitskell, “Measurements of wavelength-dependent double photoelectron emission from single photons in vuv-sensitive photomultiplier tubes,” Journal of Instrumentation **10**, P09010 (2015).
[11] D. Q. Huang, Ultra-Low Energy Calibration of the LUX and LZ Dark Matter Detectors, Ph.D. thesis, Brown University (2020).
[12] D. S. Akerib *et al.* (LUX Collaboration), “First results from the LUX dark matter experiment at the Sanford Underground Research Facility,” Phys. Rev. Lett. **112**, 091303 (2014).
[13] D. S. Akerib *et al.* (LUX), “Results from a search for dark matter in the complete LUX exposure,” Phys. Rev. Lett. **118**, 021303 (2017), arXiv:1608.07648 [astro-ph.CO].
[14] D. S. Akerib *et al.* (LUX Collaboration), “Results on the Spin-Dependent Scattering of Weakly Interacting Massive Particles on Nucleons from the Run 3 Data of the LUX Experiment,” Phys. Rev. Lett. **116**, 161302 (2016).
[15] D. S. Akerib *et al.* (LUX), “Results of a Search for Sub-GeV Dark Matter Using 2013 LUX Data,” Phys. Rev. Lett. **122**, 131301 (2019), arXiv:1811.11241 [astro-ph.CO].
[16] D. S. Akerib *et al.* (LUX), “First direct detection constraint on mirror dark matter kinetic mixing using LUX 2013 data,” Phys. Rev. D **101**, 012003 (2020),

arXiv:1908.03479 [hep-ex].

[17] D. S. Akerib *et al.* (LUX), "First Searches for Axions and Axionlike Particles with the LUX Experiment," Phys. Rev. Lett. **118**, 261301 (2017), arXiv:1704.02297 [astro-ph.CO].

[18] D. S. Akerib *et al.* (LUX), "Ultralow energy calibration of LUX detector using ^{127}Xe electron capture," Phys. Rev. **D96**, 112011 (2017), arXiv:1709.00800 [physics.ins-det].

[19] D. S. Akerib *et al.* (LUX Collaboration), "Tritium calibration of the lux dark matter experiment," Phys. Rev. D **93**, 072009 (2016).

[20] D. S. Akerib *et al.* (LUX), "Investigation of background electron emission in the LUX detector," Phys. Rev. D **102**, 092004 (2020), arXiv:2004.07791 [physics.ins-det].

[21] M. Szydagis *et al.*, "Noble Element Simulation Technique v2.0," (2018), version 2.0.0, 10.5281/zenodo.1314669.

[22] D. S. Akerib *et al.*, "LUXSim: A Component-Centric Approach to Low-Background Simulations," Nucl. Instrum. Meth. **A675**, 63–77 (2012), arXiv:1111.2074 [physics.data-an].

[23] C. S. Amarasinghe, R. Coronel, D. Q. Huang, Y. Liu, M. Arthurs, S. Steinfeld, W. Lorenzon, and R. Gaitskell, "Feasibility study to use neutron capture for an ultralow energy nuclear-recoil calibration in liquid xenon," Phys. Rev. D **106**, 032007 (2022), arXiv:2204.03109 [physics.ins-det].

[24] D. S. Akerib *et al.* (LUX), "3D Modeling of Electric Fields in the LUX Detector," JINST **12**, P11022 (2017), arXiv:1709.00095 [physics.ins-det].

[25] P. Sorensen *et al.*, "The scintillation and ionization yield of liquid xenon for nuclear recoils," Nuclear Instruments and Methods in Physics Research Section A: Accelerators, Spectrometers, Detectors and Associated Equipment **601**, 339 – 346 (2009).

[26] D. S. Akerib *et al.* (LUX), "Calibration, event reconstruction, data analysis, and limit calculation for the LUX dark matter experiment," Phys. Rev. **D97**, 102008 (2018), arXiv:1712.05696 [physics.ins-det].

[27] D. S. Akerib *et al.*, "LUX trigger efficiency," Nucl. Instrum. Meth. **A908**, 401–410 (2018), arXiv:1802.07784 [physics.ins-det].

[28] B.G. Lenardo *et al.*, "Low-Energy Physics Reach of Xenon Detectors for Nuclear-Recoil-Based Dark Matter and Neutrino Experiments," Phys. Rev. Lett. **123**, 231106 (2019).

[29] Peter Sorensen and Carl Eric Dahl, "Nuclear recoil energy scale in liquid xenon with application to the direct detection of dark matter," Phys. Rev. D **83**, 063501 (2011), arXiv:1101.6080 [astro-ph.IM].

[30] J Lindhard, M Scharff, and H E Schioett, "Range concepts and heavy ion ranges (notes on atomic collisions, ii)," Kgl. Danske Videnskab. Selskab. Mat. Fys. Medd. **Vol: 33: No. 14** (1963).

[31] Carl Eric Dahl, The physics of background discrimination in liquid xenon, and first results from Xenon10 in the hunt for WIMP dark matter, Ph.D. thesis, Princeton U. (2009).

[32] E. Aprile *et al.* (XENON), "Search for Coherent Elastic Scattering of Solar ^{8}B Neutrinos in the XENON1T Dark Matter Experiment," Phys. Rev. Lett. **126**, 091301 (2021), arXiv:2012.02846 [hep-ex].

[33] Wenbo Ma *et al.* (PandaX), "Search for Solar B8 Neutrinos in the PandaX-4T Experiment Using Neutrino-Nucleus Coherent Scattering," Phys. Rev. Lett. **130**, 021802 (2023), arXiv:2207.04883 [hep-ex].

[34] Ciaran A. J. O'Hare, "New Definition of the Neutrino Floor for Direct Dark Matter Searches," Phys. Rev. Lett. **127**, 251802 (2021), arXiv:2109.03116 [hep-ph].

[35] J. D. Lewin and P. F. Smith, "Review of mathematics, numerical factors, and corrections for dark matter experiments based on elastic nuclear recoil," Astropart. Phys. **6**, 87–112 (1996).

[36] M. Szydagis *et al.*, "NESTCollaboration/nest: New, flexible LXe NR yields and resolution model + G4 improvements + linear Noise + much more," (2022), version 2.3.11, 10.5281/zenodo.7061832.

[37] D. S. Akerib *et al.* (LUX), "Extending light WIMP searches to single scintillation photons in LUX," Phys. Rev. D **101**, 042001 (2020), arXiv:1907.06272 [astro-ph.CO].

[38] D. S. Akerib *et al.*, "Enhancing the sensitivity of the LUX-ZEPLIN (LZ) dark matter experiment to low energy signals," (2021), arXiv:2101.08753 [astro-ph.IM].

[39] Elena Aprile *et al.* (XENON), "First Indication of Solar B8 Neutrinos via Coherent Elastic Neutrino-Nucleus Scattering with XENONnT," Phys. Rev. Lett. **133**, 191002 (2024), arXiv:2408.02877 [nucl-ex].

[40] Zihao Bo *et al.* (PandaX), "First Indication of Solar B8 Neutrinos through Coherent Elastic Neutrino-Nucleus Scattering in PandaX-4T," Phys. Rev. Lett. **133**, 191001 (2024), arXiv:2407.10892 [hep-ex].

[41] Chang Cai *et al.* (RELICS), "Reactor neutrino liquid xenon coherent elastic scattering experiment," Phys. Rev. D **110**, 072011 (2024), arXiv:2405.05554 [hep-ex].

[42] Kate Scholberg, "Prospects for measuring coherent neutrino-nucleus elastic scattering at a stopped-pion neutrino source," Phys. Rev. D **73**, 033005 (2006), arXiv:hep-ex/0511042.